

# A method of an on-demand beamsplitter for trapped-ion quantum computers

Takanori Nishi\*

*Institute for Attosecond Laser Facility, The University of Tokyo,  
7-3-1 Hongo, Bunkyo-ku, Tokyo 113-0033, Japan*

(Dated: August 28, 2025)

Quantum information processing using local modes of trapped ions has been applied to implementing bosonic quantum error correction codes and conducting efficient quantum simulation of bosonic systems. However, control of entanglement among local modes remains difficult because entanglement among resonant local modes is governed by the Coulomb interaction, which is not switchable. We propose a method of a beamsplitter for a trapped-ion architecture, where the secular frequency of each mode is dynamically controllable. The neighboring modes are far detuned except when the beamsplitter needs to be applied to them. We derive the analytical formula of the proposed procedure and numerically confirm its validity.

## I. INTRODUCTION

Continuous variable (CV) encoding of quantum information processing (QIP) provides an efficient way of constructing quantum error correction such as the Gottesman–Kitaev–Preskill (GKP) codes [1] and the cat codes [2, 3] as well as simulation of bosonic systems [4–8]. The initialization and the error-correction cycle of the GKP codes have been demonstrated in trapped ions [9, 10] and in superconducting circuits [11, 12]. For trapped ions, a universal gate set for the GKP code has been realized in Ref. [13], where two GKP qubits are encoded using two local modes of a single ion. All of the logical gates are implemented by modulating phases of sideband lasers. Because a single ion can accommodate only three local modes, a novel scheme for entangling local modes of different ions needs to be developed in order to achieve a large scale of CV-QIP. However, the control of entanglement among local modes of different ions is difficult because the entanglement of local modes is generated by phonon hopping induced by the Coulomb interaction, i.e., the entangling gate cannot be turned off even if it is not needed. Because the Hamiltonian of phonon hopping is equivalent to that of a beamsplitter, phonon hopping can be regarded as a "non-on-demand beamsplitter."

Phonon hopping into a given mode can be suppressed if transition frequencies of the mode are far detuned from those of the other modes. By illuminating an ion with a laser light resonant with a red sideband, the internal and the motional states of the ion become coupled and the transition frequencies of the coupled state are shifted from those without laser light so that hopping from the other modes into the illuminated mode is suppressed, which is called a phonon blockade [14, 15]. Because the state of the mode driven by laser is disturbed unless it is in the ground state, the phonon blockade is only applicable to the state preparation or the state detection but not to the gate operation.

In order to suppress phonon hopping through the entire execution of a quantum circuit or an analog quantum simulation, we can use the fact that the rate of hopping  $\kappa$  depends on the distance between ions  $d$  as  $\kappa \propto d^{-3}$ . By leveraging the recent developments of highly accurate ion transport using quantum charge-coupled devices [16], phonon hopping can be suppressed by storing the ions with keeping the distance between them sufficiently large, while phonon hopping can be induced by transporting two ions in close proximity, deforming the trap potential to accelerate phonon hopping, and separating them again. Lau and James [17] showed that the beamsplitter as well as Gaussian and non-Gaussian single-mode operations can be implemented by combining the modulation of trap potential and the ion transport, and thus the universal gate set for CV encoding can be constructed without laser.

We can also suppress phonon hopping without ion transport by using the dynamical decoupling (DD) [18, 19], where all the modes are resonant and phonon hopping proceeds among all the modes. Control of hopping is achieved by applying a sequence of  $\pi$ -phase shift ( $P_\pi$ ) gates to a set of modes so that undesirable hopping is canceled at the end of the sequence. The fidelity of cancellation decreases as the duration of the  $P_\pi$  gate increases because phonon hopping proceeds even during the  $P_\pi$  gate, which degrades the fidelity of the  $P_\pi$  gate. A fast  $P_\pi$  gate can be implemented by modulating the trap potential as demonstrated in Ref. [20], with which we are able to cancel phonon hopping and implement multi-mode entangling gates with high fidelity by a method called the cancellation of Coulomb coupling by modulating harmonic potential (C3PO) [21].

In the present study, we propose an on-demand beamsplitter by controlling the detuning of each mode using a frequency-conversion method within a few microseconds. The present method does not change the population of any modes unlike the phonon blockade or need any gate operation to cancel phonon hopping unlike the DD. We derive the analytical formula of the procedure and confirm its validity by numerical simulation.

\* nishi@chem.s.u-tokyo.ac.jp

## II. METHOD

### A. A chain of detuned local modes

We consider a chain of ions and assume that the secular frequency along the radial direction  $X$  of each ion is a few MHz while the hopping rate is a few kHz or less. Therefore, for a chain of  $M$  ions, we can consider  $M$  local modes along the  $X$  direction. The Hamiltonian for such a chain of ions under the rotating-wave approximation is given by Eq. (A3). We assume that the ions are trapped by a surface electrode trap and the secular frequency of the  $j$ th mode can be controlled as  $\omega_j(t)$  by modulating the DC voltage applied to the electrodes as demonstrated in Ref. [20]. The Hamiltonian of the chain of ions with mass  $m$  is given by

$$H(t) = H_0 + \sum_j \frac{\hbar\Omega_j^2(t)}{4\omega_j} (a_{j,\omega_j}^\dagger + a_{j,\omega_j})^2 \quad (1)$$

$$H_0 = \sum_j \hbar\omega_j \left( a_{j,\omega_j}^\dagger a_{j,\omega_j} + \frac{1}{2} \right) + \sum_{j>k} \frac{\hbar\kappa_{j,k}}{2} (a_{j,\omega_j}^\dagger a_{k,\omega_k} + a_{j,\omega_j} a_{k,\omega_k}^\dagger), \quad (2)$$

where  $H_0$  is the Hamiltonian of the ion chain without any modulation of the DC voltage and each mode has static secular frequency  $\omega_j$ ,  $\kappa_{j,k}$  is the rate of hopping between the  $j$ th and the  $k$ th modes, and  $\Omega_j^2(t) \equiv \omega_j^2(t) - \omega_j^2$ . The lowering (raising) operator  $a_{j,\omega_j}$  ( $a_{j,\omega_j}^\dagger$ ) of the  $j$ th mode is defined with respect to the  $j$ th coordinate scaled by  $x_{0,j} = \sqrt{\hbar/(m\omega_j)}$ .

In the following, we assume that three values of secular frequency are available; two “memory frequencies”  $\omega_l$  and  $\omega_h$ , and a “gate frequency”  $\omega_m$ , where they satisfy  $\omega_l < \omega_m < \omega_h$  and the detunings,  $\delta_{hm} = \omega_h - \omega_m$  and  $\delta_{ml} = \omega_m - \omega_l$ , are sufficiently large so that phonon hopping is negligible between the modes oscillating at different frequencies. The gate frequency  $\omega_m$  is used only for the implementation of the beamsplitter as we discuss later. In order to suppress phonon hopping between the neighboring modes, we choose  $\omega_j = \omega_h$  for even  $j$  and  $\omega_j = \omega_l$  for odd  $j$ .

In this configuration, we still suffer from phonon hopping between the  $j$ th and the  $k$ th modes when  $|j - k|$  is even. There are two schemes for suppressing phonon hopping among non-neighboring modes. In the first scheme, we assume that other values of frequency are available, e.g., if we can use  $\omega'$ , which is far detuned from any other frequencies and satisfying  $\omega' < \omega_l$ , we set the frequency of  $j$ th mode to  $\omega_h$ ,  $\omega_l$ , or  $\omega'$  for  $j = 0, 1$ , or  $2 \pmod{3}$ , respectively, so that any pair of modes satisfying  $|j - k| \leq 2$  becomes off-resonant and hopping between them is negligible. In the other scheme, we apply the C3PO to non-neighboring modes. Due to the relation  $\kappa \propto d^{-3}$ , the hopping rate between the modes with  $|j - k|$  is  $|j - k|^3$  times smaller than that between the neighboring modes.

Moreover, because we only need to consider the pair with even  $|j - k|$ , the hopping rate of the relevant pairs of modes scales as  $\propto (2n)^{-3}$  with  $n \in \mathbb{N}$ . Therefore, the number of  $P_\pi$  gates needed to implement the C3PO is much smaller than that for the original proposal of the C3PO [21].

The entanglement between neighboring modes can be generated in three steps; (1) the frequency conversion (FC) of each mode to  $\omega_m$ , which we denote as  $FC(\omega \rightarrow \omega_m)$ , (2) phonon hopping, and (3) the inverse FC (iFC) back to the memory frequency,  $iFC(\omega_m \rightarrow \omega)$ . For example, when we have two modes with  $\omega_0 = \omega_h$  and  $\omega_1 = \omega_l$ , we first apply the down conversion  $FC_0(\omega_h \rightarrow \omega_m)$  and the up conversion  $FC_1(\omega_l \rightarrow \omega_m)$ . Because the resulting states are resonant, phonon hopping proceeds. Finally, once the desired amount of entanglement is generated, we apply the iFC,  $iFC_0(\omega_m \rightarrow \omega_h)$  and  $iFC_1(\omega_m \rightarrow \omega_l)$ . Unlike the C3PO, the proposed scheme does not need to cancel unwanted entanglement and provides an entangling gate only when we need it, and thus we call the scheme the on-demand beamsplitter.

As we show in II C, the above procedure is equivalent to a beamsplitter sandwiched by the additional phase-shift gates. Because the phase-shift gate can be implemented by sequentially applying FC and iFC as shown in Eq. (22), we can cancel the additional phase shift if needed by applying the phase-shift gates before and after the on-demand beamsplitter.

### B. Time evolution in the Heisenberg picture

In the following, we consider two ions with  $\omega_0 = \omega_h$  and  $\omega_1 = \omega_l$  and the three steps of the on-demand beamsplitter; (1) FC to  $\omega_m$  from  $t = 0$  to  $t = T_1 = T_{FC}$ , (2) phonon hopping for the duration  $T_B$ , i.e., from  $t = T_1$  to  $t = T_2 = T_{FC} + T_B$ , and (3) iFC from  $t = T_2$  to  $t = T_3 = 2T_{FC} + T_B$ . First, we derive the time evolution during FC in the Heisenberg picture by using the Lewis–Riesenfeld theory [22] (see Appendix C) of a time-dependent harmonic oscillator (TDHO) defined by the Hamiltonian  $H(t) = P^2/(2m) + m\omega^2(t)X^2/2$ . We denote the initial and the final frequencies by the subscript of  $\omega(t)$  as well as the corresponding  $b(t)$  defined by Eq. (C3), e.g.,  $\omega_{hm}(t)$  and  $b_{hm}(t)$  for  $FC_0(\omega_h \rightarrow \omega_m)$ . By neglecting hopping between the 0th and the 1st modes and using Eq. (D5), we obtain the raising and the lowering operators after the FC as  $\mathbf{a}_{mm}(T_1) = S_{FC,hm,lm} \mathbf{a}_{hl}$ , where

$$\mathbf{a}_{mm}(T_1) = \begin{bmatrix} a_{0,\omega_m}(T_1) \\ a_{0,\omega_m}^\dagger(T_1) \\ a_{1,\omega_m}(T_1) \\ a_{1,\omega_m}^\dagger(T_1) \end{bmatrix}, \quad \mathbf{a}_{hl} = \begin{bmatrix} a_{0,\omega_h} \\ a_{0,\omega_h}^\dagger \\ a_{1,\omega_l} \\ a_{1,\omega_l}^\dagger \end{bmatrix}, \quad (3)$$

$$S_{FC,hm,lm} = \begin{bmatrix} S_{hm} & O \\ O & S_{lm} \end{bmatrix}. \quad (4)$$

$S_{hm}$  and  $S_{lm}$  are obtained by substituting  $\omega_i = \omega_h$  or  $\omega_l$ ,  $\omega_f = \omega_m$ , and  $b(t) = b_{hm}(t)$  or  $b_{lm}(t)$  in Eqs. (C7), (C9),

and (C10).

The effect of hopping during FC can be relevant when the secular frequencies of the two modes become close. However, such an effect can be suppressed by setting the duration  $T_{\text{FC}}$  much smaller than the hopping time scale  $\propto \kappa_{0,1}^{-1}$  and therefore we expect that Eq. (3) can well approximate the time evolution under Eq. (1).

In the second step, we keep the frequency of both modes at  $\omega(t) = \omega_m$  for the duration  $T_B$  to induce the desired amount of hopping, during which the Hamiltonian becomes simple as

$$\begin{aligned} H(t) &\equiv H_B \\ &= \sum_{j=0,1} \hbar \omega_m \left( a_{j,\omega_m}^\dagger a_{j,\omega_m} + \frac{1}{2} \right) \\ &\quad + \frac{\hbar \tilde{\kappa}_{0,1}}{2} \left( a_{0,\omega_m}^\dagger a_{1,\omega_m} + a_{0,\omega_m} a_{1,\omega_m}^\dagger \right), \end{aligned} \quad (5)$$

where  $\tilde{\kappa}_{0,1} = e^2/(4\pi\epsilon_0 d_{0,1}^3 m \omega_m)$ . The time evolution with this Hamiltonian is well known. In the interaction frame (IF) with respect to  $\sum_j \hbar \omega_m (a_{j,\omega_m}^\dagger a_{j,\omega_m} + 1/2)$ , the propagator  $\exp(-iH_B^{\text{IF}} T_B/\hbar)$  coincides with the unitary operator representing a beamsplitter  $U_B = \exp(-i\theta(a_0^\dagger a_1 + a_0 a_1^\dagger))$  with  $\theta = \tilde{\kappa}_{0,1} T_B/2$ . Therefore, the output of the second step in the IF is given by  $\mathbf{a}_{mm}^{\text{IF}}(T_2) = B(\theta) \mathbf{a}_{mm}(T_1)$ , where

$$B(\theta) = \begin{bmatrix} \cos \theta & 0 & -i \sin \theta & 0 \\ 0 & \cos \theta & 0 & i \sin \theta \\ -i \sin \theta & 0 & \cos \theta & 0 \\ 0 & i \sin \theta & 0 & \cos \theta \end{bmatrix}. \quad (6)$$

In order to take into account the dynamical phase, we define the transformation matrix for the phase-shift gates on two modes as

$$P(\phi_1, \phi_2) = \begin{bmatrix} e^{-i\phi_1} & 0 & 0 & 0 \\ 0 & e^{i\phi_1} & 0 & 0 \\ 0 & 0 & e^{-i\phi_2} & 0 \\ 0 & 0 & 0 & e^{i\phi_2} \end{bmatrix}, \quad (7)$$

and obtain  $\mathbf{a}_{mm}(T_2) = P(\omega_m T_B, \omega_m T_B) \mathbf{a}_{mm}^{\text{IF}}(T_2)$ .

In the third step, we apply iFC as  $\mathbf{a}_{hl}(T_3) = S_{\text{FC},mh,ml} \mathbf{a}_{mm}(T_2)$ , where

$$S_{\text{FC},mh,ml} = \begin{bmatrix} S_{mh} & O \\ O & S_{ml} \end{bmatrix} \quad (8)$$

The  $2 \times 2$  matrices  $S_{mh}$  and  $S_{ml}$  are defined by using  $\omega_i = \omega_m$  and  $\omega_j = \omega_h$  or  $\omega_l$ .

### C. Simplification in the frequency conversion

In deriving Eq. (D5), we imposed the boundary conditions  $b(t_i) = 1$  and  $\dot{b}(t_i) = 0$ . In addition, we impose  $b(t_f) = \sqrt{\omega_i/\omega_f}$  and  $\dot{b}(t_f) = 0$  so that we obtain

$\eta(t_f) = 1$  and  $\zeta(t_f) = 0$ , with which Eq. (D5) is rewritten as

$$S_{if} = \begin{bmatrix} e^{i\Theta(t_f)} & 0 \\ 0 & e^{-i\Theta(t_f)} \end{bmatrix}. \quad (9)$$

These conditions correspond to the requirement for  $\omega(t)$  to be smooth at  $t_i$  and  $t_f$ . From Eq. (9), the output of FC can be written as

$$a_{\omega_f}(t_f) = a_{\omega_i} e^{i\Theta(t_f)}, \quad (10)$$

which means that FC preserves the population in the Fock basis and is equivalent to the phase-shift gate. On the other hand, if we describe the output of FC in terms of the  $|n; \omega_i\rangle$  basis, Eq. (10) can be rewritten as

$$a_{\omega_i}(t_f) = a_{\omega_i} e^{i\Theta(t_f)} \cosh r - a_{\omega_i}^\dagger e^{-i\Theta(t_f)} \sinh r, \quad (11)$$

where  $r = \log \sqrt{\omega_f/\omega_i}$ . This means that FC is the combination of the phase shift and the squeezing with  $r$  the squeezing strength.

The unitary operator corresponding to Eq. (10) can be written as

$$U_{\text{FC}}(\Theta(t_f)) = \sum_n e^{i\Theta(t_f)(n+1/2)} |n; \omega_f\rangle \langle n; \omega_i|. \quad (12)$$

It is well known that such a population transfer can be realized if the modulation of the Hamiltonian is slow so that the adiabatic approximation is valid, however, because we have not made any assumption on the time scale of FC, the duration  $T_{\text{FC}}$  can be arbitrarily small as long as  $\omega(t)$  defined by Eq. (C4) is real and  $b(t)$  and  $\dot{b}(t)$  satisfy the above boundary conditions.

The entire procedure of the on-demand beamsplitter in the Heisenberg picture can thus be written as

$$\begin{aligned} \mathbf{a}_{hl}(T_3) &= S_{\text{FC},mh,ml} P(\omega_m T_B, \omega_m T_B) B(\theta) S_{\text{FC},mh,ml} \mathbf{a}_{hl} \\ &= P(-\Theta_{mh}, -\Theta_{ml}) P(\omega_m T_B, \omega_m T_B) B(\theta) \\ &\quad \times P(-\Theta_{hm}, -\Theta_{lm}) \mathbf{a}_{hl} \\ &= P(-\Theta_{mh} + \omega_m T_B, -\Theta_{ml} + \omega_m T_B) B(\theta) \\ &\quad \times P(-\Theta_{hm}, -\Theta_{lm}) \mathbf{a}_{hl}. \end{aligned} \quad (13)$$

In the IF with respect to  $\sum_j \hbar \omega_j (a_{j,\omega_j}^\dagger a_{j,\omega_j} + 1/2)$ , we obtain

$$\mathbf{a}_{hl}^{\text{IF}}(T_3) = P(-\omega_h T_3, -\omega_l T_3) \mathbf{a}_{hl}(T_3), \quad (14)$$

and we summarize the transformation matrix for the entire process in the IF as

$$\begin{aligned} S_{\text{ODB}}^{\text{IF}}(\theta) &= P(-\Theta_{mh} + \omega_m T_B - \omega_h T_3, -\Theta_{ml} + \omega_m T_B - \omega_l T_3) \\ &\quad \times B(\theta) P(-\Theta_{hm}, -\Theta_{lm}). \end{aligned} \quad (15)$$

### III. RESULTS

We demonstrate the on-demand beamsplitter for two cases; the 50:50 beamsplitter and the SWAP gate. We solve the time-dependent Schrödinger equation (TDSE) numerically using time-dependent variational principle with the matrix-product state (TDVP-MPS) [23, 24], which we implement using a Python package `mpsqd` [25]. Although we use the second quantization in deriving the analytical expressions, we adopt the first quantization for the numerical simulation because it is straightforward to describe the GKP states. The state vectors are represented in  $x$  coordinate using 128 grid points for each mode and the operators are represented using  $x$  and  $p$  such as Eqs. (A2) and (A4).

We consider two  $^{40}\text{Ca}^+$  ions and their local modes along the  $X$  direction. We set the memory frequencies to  $\omega_h = 2\pi \times 2.64$  MHz and  $\omega_l = 2\pi \times 2.20$  MHz, respectively, and the gate frequency to  $\omega_m = 2\pi \times 2.42$  MHz. By simulating the propagation under the bare Hamiltonian defined by Eq. (2), we have confirmed that hopping between two modes is negligible if  $\omega_j \neq \omega_k$  and  $\omega_j, \omega_k \in \{\omega_h, \omega_m, \omega_l\}$ , and then we set  $\omega_0 = \omega_h$  and  $\omega_1 = \omega_l$ . The distance between ions is set to  $43.8\ \mu\text{m}$ , which corresponds to  $\tilde{\kappa}_{0,1} = 0.432$  kHz. For FC, we define the following functions,

$$f_u(g, t) = 1 - \frac{g}{2} \left( 1 + \text{erf} \left[ \left( \frac{t}{T_{\text{FC}}} - \frac{1}{2} \right) \sigma \right] \right) \quad (16)$$

$$f_d(g, t) = 1 + \frac{g}{2} \left( 1 + \text{erf} \left[ \left( \frac{t}{T_{\text{FC}}} - \frac{1}{2} \right) \sigma \right] \right), \quad (17)$$

and the  $b(t)$  function as  $b(t) = f_u(1 - \sqrt{\omega_i/\omega_f}, t)$  for the up conversion ( $\omega_i < \omega_f$ ) while  $b(t) = f_d(\sqrt{\omega_i/\omega_f} - 1, t)$  for the down conversion ( $\omega_i > \omega_f$ ). With this definition of  $b(t)$ , the phases for the up conversion and the down conversion for each mode are the same, i.e.,  $\Theta_{hm} = \Theta_{mh}$  and  $\Theta_{lm} = \Theta_{ml}$ . We set the duration of FC to  $T_{\text{FC}} = 4\ \mu\text{s}$  and the width of the error function to  $\sigma = 6$ , and so the rate of FC in the present study is  $(\omega_h - \omega_m)/T_{\text{FC}} = 2\pi \times 55\ \text{kHz}/\mu\text{s}$ , which is comparable to the rate  $2\pi \times 57\ \text{kHz}/\mu\text{s}$  demonstrated in Ref. [20]. Fig. 1 shows  $\omega(t)$  and  $b(t)$  for  $\text{FC}_0(\omega_h \rightarrow \omega_m)$  and  $\text{FC}_1(\omega_l \rightarrow \omega_m)$ .

We note that these parameters satisfy the adiabatic condition as shown in Appendix E. However, because we derived the analytical formula (15) without adiabatic approximation, the on-demand beamsplitter can be implemented with much faster modulation of  $\omega(t)$ , e.g., with shorter  $T_{\text{FC}}$  and/or larger  $g$ .

In order to analyze the time evolution by phonon hopping in the Schrödinger picture, we use the following re-

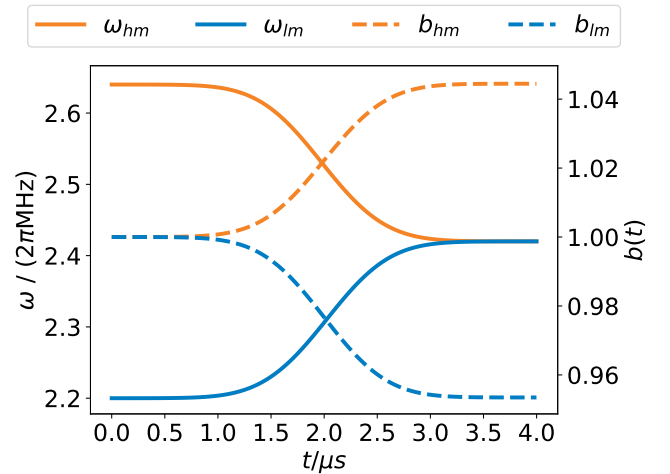


FIG. 1.  $b(t)$  (dashed lines) for the up (blue) and down (orange) conversions defined by Eq. (16) and (17), respectively. The corresponding  $\omega(t)$  (solid lines) is defined by Eq. (C4).

lation,

$$\begin{aligned} U_B(\theta) |j\rangle_1 |k\rangle_0 &= U_B \left( a_1^\dagger \right)^j \left( a_0^\dagger \right)^k U_B^\dagger U_B |0\rangle_1 |0\rangle_0 \\ &= \left( a_1^\dagger \cos \theta - i a_0^\dagger \sin \theta \right)^j \\ &\quad \times \left( -i a_1^\dagger \sin \theta + a_0^\dagger \cos \theta \right)^k |0\rangle_1 |0\rangle_0. \end{aligned} \quad (18)$$

We define the unitary operators for the two-mode FC and iFC as

$$\begin{aligned} U_{\text{FC}}(\phi_0, \phi_1) &= U_{\text{FC}_1}(\phi_1) U_{\text{FC}_0}(\phi_0) \\ &= \sum_j e^{i\phi_1(j+1/2)} |j; \omega_m\rangle_1 \langle j; \omega_l|_1 \\ &\quad \otimes \sum_k e^{i\phi_0(k+1/2)} |k; \omega_m\rangle_0 \langle k; \omega_h|_0 \end{aligned} \quad (19)$$

$$\begin{aligned} U_{i\text{FC}}(\phi_0, \phi_1) &= \sum_j e^{i\phi_1(j+1/2)} |j; \omega_l\rangle_1 \langle j; \omega_m|_1 \\ &\quad \otimes \sum_k e^{i\phi_0(k+1/2)} |k; \omega_h\rangle_0 \langle k; \omega_m|_0, \end{aligned} \quad (20)$$

respectively, and for the two-mode phase-shift gate as

$$\begin{aligned} U_{\text{P}}(\phi_0, \phi_1) &= \sum_j e^{-i\phi_1(j+1/2)} |j; \omega\rangle_1 \langle j; \omega|_1 \\ &\quad \otimes \sum_k e^{-i\phi_0(k+1/2)} |k; \omega'\rangle_0 \langle k; \omega'|_0, \end{aligned} \quad (21)$$

where  $\omega$  and  $\omega'$  are the frequency of the state  $U_{\text{P}}$  acts on. We note that the kets are labeled from the right while the parameters of the two-mode gates in Eqs. (7), (19), (20), and (21) are labeled from the left. We also note that the phase-shift gate can be constructed by sequentially

applying FC and *iFC*, e.g.,

$$\begin{aligned} U_{\text{P}_0}(\phi_a + \phi_b) &= \sum_k e^{-i(\phi_a + \phi_b)(k+1/2)} |k; \omega_h\rangle_0 \langle k; \omega_h|_0 \\ &= U_{i\text{FC}_0}(-\phi_b) U_{\text{FC}_0}(-\phi_a). \end{aligned} \quad (22)$$

### A. The Hong–Ou–Mandel effect

The 50:50 beamsplitter is realized by setting  $\theta = \pi/4$ , which corresponds to  $T_B = 579 \mu\text{s}$ . When the input to the 50:50 beamsplitter is  $|1\rangle_1 |1\rangle_0$ , the output is given by

$$\begin{aligned} U_B(\pi/4) |1\rangle_1 |1\rangle_0 &= \frac{1}{2} (a_1^\dagger - ia_0^\dagger) (-ia_1^\dagger + a_0^\dagger) |0\rangle_1 |0\rangle_0 \\ &= \frac{-i}{\sqrt{2}} (|2\rangle_1 |0\rangle_0 + |0\rangle_1 |2\rangle_0), \end{aligned} \quad (23)$$

which is known as the Hong–Ou–Mandel effect [26]. From Eq. (14), the output of the on-demand beamsplitter is given by

$$\begin{aligned} |\psi_{\text{HOM}}\rangle &= U_{\text{ODB}}\left(\frac{\pi}{4}\right) |1; \omega_l\rangle_1 |1; \omega_h\rangle_0 \\ &= U_{i\text{FC}}(-\Theta_{hm} + \omega_m T_B - \omega_h T_3, -\Theta_{lm} + \omega_m T_B - \omega_l T_3) \\ &\quad \times U_B(\pi/4) U_{\text{FC}}(-\Theta_{hm}, -\Theta_{lm}) |1; \omega_l\rangle_1 |1; \omega_h\rangle_0 \\ &= \frac{-i}{\sqrt{2}} (e^{i\phi_{2,0}} |2; \omega_l\rangle_1 |0; \omega_h\rangle_0 + e^{i\phi_{0,2}} |0; \omega_l\rangle_1 |2; \omega_h\rangle_0), \end{aligned} \quad (24)$$

where

$$\begin{aligned} \phi_{2,0} &= \left(\frac{1}{2}\Theta_{hm} + \frac{5}{2}\Theta_{lm}\right) - 3\omega_m T_B \\ &\quad + \left(\frac{1}{2}\omega_h + \frac{5}{2}\omega_l\right) T_3 + \frac{3}{2}(\Theta_{hm} + \Theta_{lm}) \end{aligned} \quad (25)$$

$$\begin{aligned} \phi_{0,2} &= \left(\frac{5}{2}\Theta_{hm} + \frac{1}{2}\Theta_{lm}\right) - 3\omega_m T_B \\ &\quad + \left(\frac{5}{2}\omega_h + \frac{1}{2}\omega_l\right) T_3 + \frac{3}{2}(\Theta_{hm} + \Theta_{lm}) \end{aligned} \quad (26)$$

In the simulation of the HOM effect, we include the hopping term in Eq. (1) even during FC and therefore the unitary operator of FC can deviate from Eq. (12). In Fig. 2, we show the population of three states involved in the HOM effect, i.e.,  $|1\rangle_1 |1\rangle_0$ ,  $|2\rangle_1 |0\rangle_0$ , and  $|0\rangle_1 |2\rangle_0$  in the memory-frequency basis (solid lines) and in the gate-frequency basis (dashed lines). In Fig. 2 (a), the gray areas at the beginning and the end represent the operation of FC and *iFC*, respectively. The expanded view during FC shown in Fig. 2 (b) clearly demonstrates the population transfer from the memory-frequency basis  $|1; \omega_l\rangle_1 |1; \omega_h\rangle_0$  to the gate-frequency basis  $|1; \omega_m\rangle_1 |1; \omega_m\rangle_0$ . The population of  $|1; \omega_l\rangle_1 |1; \omega_h\rangle_0$  at the end of FC as well as that of  $|1; \omega_m\rangle_1 |1; \omega_m\rangle_0$  at the beginning of FC equals to the overlap between them  $|\langle 1; \omega_l | 1; \omega_m \rangle \langle 1; \omega_h | 1; \omega_m \rangle|^2 = 0.994$ . As shown in Fig. 2 (c), the HOM effect can be observed in

the gate-frequency basis at the end of  $U_B$ , i.e., the population of  $|2; \omega_m\rangle_1 |0; \omega_m\rangle_0$  and  $|0; \omega_m\rangle_1 |2; \omega_m\rangle_0$  are 0.5 at  $t = 583 \mu\text{s}$ . The population of these states are then transferred to the memory-frequency basis,  $|2; \omega_l\rangle_1 |0; \omega_h\rangle_0$  and  $|0; \omega_l\rangle_1 |2; \omega_h\rangle_0$ , at the end of *iFC* at  $t = 587 \mu\text{s}$ .

By denoting the final state of the simulation as  $|\psi_{\text{sim}}\rangle$ , the infidelity defined as  $1 - |\langle \psi_{\text{HOM}} | \psi_{\text{sim}} \rangle|^2$  is  $1.15 \times 10^{-4}$ . Even if we neglect the hopping term during FC and *iFC*, the infidelity is  $2.58 \times 10^{-5}$  due to the numerical error in the TDVP-MPS simulation and therefore we estimate the effect of the hopping term during FC and *iFC* by the increase of the infidelity,  $8.92 \times 10^{-5}$ .

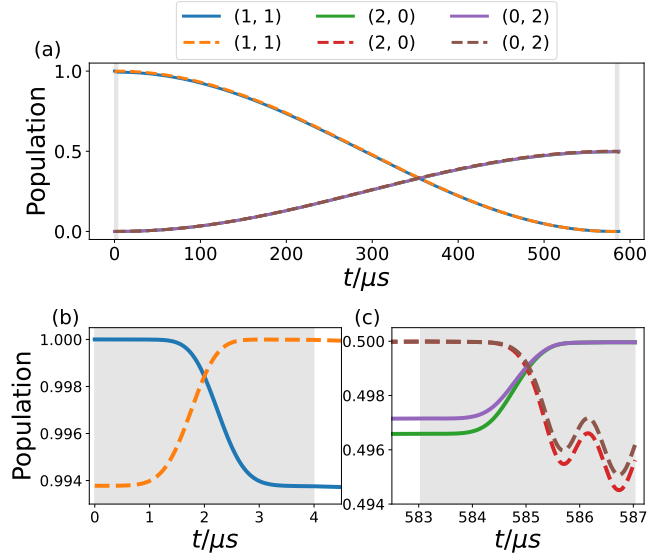


FIG. 2. (a) The populations of three states relevant in the HOM effect,  $|1\rangle_1 |1\rangle_0$ ,  $|2\rangle_1 |0\rangle_0$ , and  $|0\rangle_1 |2\rangle_0$  in the memory-frequency basis (solid lines) and the gate-frequency basis (dashed lines) (b) and (c) shows the expanded view during FC and *iFC*, respectively.

### B. SWAP the GKP states

The logical two-qubit gates for the finite-energy GKP codes suffer from the error caused by the finite squeezing of the GKP states. Rojkov *et al.* proposed to combine SWAP gates and qutrit-controlled unitary gates to implement a controlled-Z gate for the finite-energy GKP codes with high fidelity [27]. Therefore, we demonstrate the SWAP gate using the on-demand beamsplitter in the following.

First, we double the duration of hopping  $T_B$  compared to the 50:50 beamsplitter, i.e., we set  $\theta = \pi/2$  and  $T_B = 1158 \mu\text{s}$ . From Eq. (18), this is not equivalent to the SWAP gate but is composed of the SWAP gate and the phase-shift

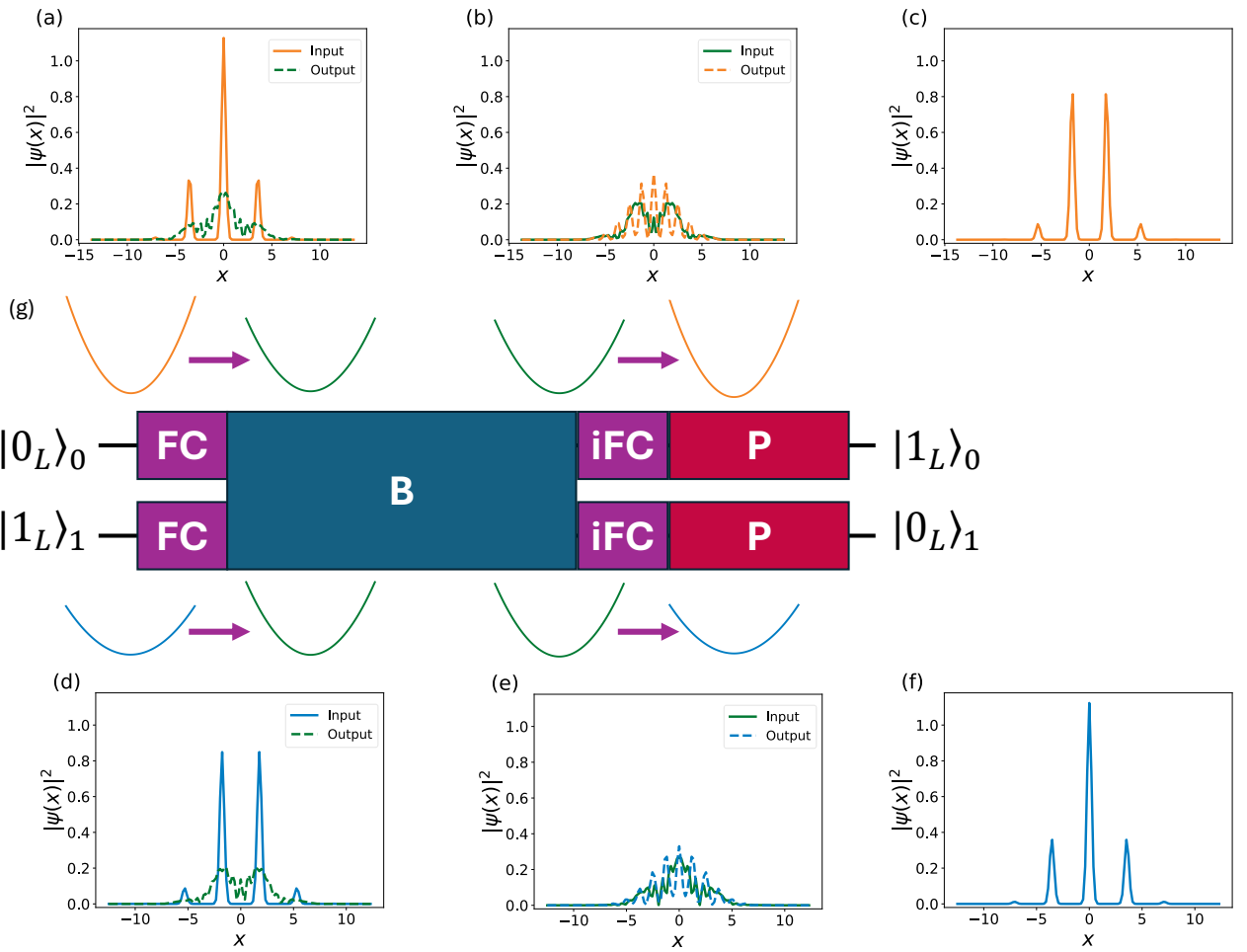


FIG. 3. The marginal distributions in the position space of each mode are shown in (a)-(f). The schematic of the on-demand beamsplitter is shown in (g), where the gates are applied from the left to right. Colors of the harmonic well and the marginal distributions correspond to the frequencies  $\omega_h$  (orange),  $\omega_m$  (green), and  $\omega_l$  (blue). The initial state is the product of GKP states  $|1_L\rangle_1 |0_L\rangle_0$  characterized by the parameters  $\Delta = \epsilon = 0.3$ . In (a) and (d) ((b) and (e)), the solid lines represent the input to FC (iFC) while the dashed lines represent the output from FC (iFC). (c) and (f) are the output of the phase-shift gate P, which completes the SWAP gate.

gate as

splitter, the output is given by

$$\begin{aligned}
 U_B(\pi/2) |j\rangle_1 |k\rangle_0 &= \left(-ia_0^\dagger\right)^j \left(-ia_1^\dagger\right)^k |0\rangle_1 |0\rangle_0 \\
 &= (-i)^{j+k} |k\rangle_1 |j\rangle_0 \\
 &= iU_P(\pi/2, \pi/2) U_{\text{SWAP}} |j\rangle_1 |k\rangle_0. \quad (27)
 \end{aligned}$$

If we input an arbitrary product state  $|\psi; \omega_l\rangle_1 |\xi; \omega_h\rangle_0 = \sum_j \alpha_j |j; \omega_l\rangle_1 \sum_k \beta_k |k; \omega_h\rangle_0$  to the on-demand beam-

$$\begin{aligned}
 &U_{\text{ODB}}\left(\frac{\pi}{2}\right) |\psi; \omega_l\rangle_1 |\xi; \omega_h\rangle_0 \\
 &= U_{i\text{FC}}(-\Theta_{hm} + \omega_m T_B - \omega_h T_3, \\
 &\quad -\Theta_{lm} + \omega_m T_B - \omega_l T_3) U_B(\pi/2) \\
 &\quad \times \sum_{j,k} \alpha_j e^{i\Theta_{lm}(j+1/2)} \beta_k e^{i\Theta_{hm}(k+1/2)} |j; \omega_m\rangle_1 |k; \omega_h\rangle_0 \\
 &= iU_{i\text{FC}}(-\Theta_{hm} + \omega_m T_B - \omega_h T_3 + \pi/2, \\
 &\quad -\Theta_{lm} + \omega_m T_B - \omega_l T_3 + \pi/2) \\
 &\quad \times \sum_{j,k} \alpha_j e^{i\Theta_{lm}(j+1/2)} \beta_k e^{i\Theta_{hm}(k+1/2)} |k; \omega_m\rangle_1 |j; \omega_h\rangle_0 \\
 &= iU_P(\phi_0, \phi_1) |\xi; \omega_l\rangle_1 |\psi; \omega_h\rangle_0, \quad (28)
 \end{aligned}$$

where

$$\begin{aligned}\phi_0 &= -(\Theta_{hm} + \Theta_{lm}) + \omega_m T_B - \omega_h T_3 + \pi/2 \\ \phi_1 &= -(\Theta_{hm} + \Theta_{lm}) + \omega_m T_B - \omega_l T_3 + \pi/2.\end{aligned}\quad (29)$$

The phase shift appeared at the last line of Eq. (28) can be compensated by applying the phase-shift gate only at the end while in the general case we need to apply the phase-shift gates at both of the beginning and the end as shown in Eq. (15). Consequently, the SWAP gate can be realized as

$$U_{\text{SWAP}} = U_{\text{P}}(-\phi_0, -\phi_1) U_{\text{ODB}}\left(\frac{\pi}{2}\right) \quad (30)$$

up to the irrelevant global phase.

We numerically simulate the SWAP gate acting on the product of finite-energy GKP states,  $|\psi_0\rangle = |1_L\rangle_1 |0_L\rangle_0 \xrightarrow{\text{SWAP}} |\psi_{\text{SWAP}}\rangle = |0_L\rangle_1 |1_L\rangle_0$ . The finite-energy GKP states in the position space are given by

$$\begin{aligned}|j_L\rangle = N_{\Delta, \epsilon} \int_{-\infty}^{\infty} dx \sum_{s \in \mathbb{Z}} & e^{-\frac{1}{2}\epsilon^2((2s+j)\sqrt{\pi})^2} \\ & \times e^{-\frac{1}{2\Delta^2}(x-(2s+j)\sqrt{\pi})^2} |x\rangle,\end{aligned}\quad (31)$$

where  $N_{\Delta, \epsilon}$  is the normalization constant,  $\Delta$  is the width of each peak, and  $\epsilon^{-1}$  is the width of the envelope. We set  $\Delta = \epsilon = 0.3$ , with which the logical infidelity of the controlled-Z gate becomes smaller than  $10^{-4}$  [27]. The sum over  $s$  is truncated at  $|s| = s_{\max} = 6$  and then  $N_{\Delta, \epsilon}$  is numerically calculated. Fig. 3 shows the marginal distribution in the position space of each mode in the memory-frequency basis,  $x_{\omega_l}$  and  $x_{\omega_h}$ . Although the populations in the Fock basis are swapped between two modes after iFC, the marginal distribution deviates from that of the logical states because of the phase shift as shown by the dashed lines in Fig. 3 (b) and (e). By applying the appropriate phase-shift gates to each mode, we can obtain the desired logical states as shown in Fig. 3 (c) and (f). The infidelity  $1 - |\langle \psi_{\text{SWAP}} | \psi_{\text{sim}} \rangle|$  is obtained as  $2.89 \times 10^{-3}$ . On the other hand, when we neglect the hopping term during FC and iFC, the infidelity caused by the numerical error is obtained as  $1.70 \times 10^{-3}$ , and therefore we estimate the effect of the hopping term by their difference,  $1.19 \times 10^{-3}$ .

#### IV. CONCLUSION

We have proposed a method for implementing an on-demand beamsplitter for trapped-ion quantum computers by combining frequency conversion, phonon hopping, and phase-shift gates. Based on the analytical solution of the time-dependent harmonic oscillator, we have derived the transformation matrix of the on-demand beamsplitter in the Heisenberg picture. Because the transformation matrix is obtained by neglecting the hopping terms during the operation of the frequency conversion, the

time-evolution under the realistic Hamiltonian can deviate from the analytical results. In order to evaluate the effect of the hopping terms, we have numerically solved the TDSE using TDVP-MPS method. The HOM effect and the SWAP of the GKP states have been successfully demonstrated. Due to the numerical error, the simulated results deviate from the analytical solution even when we neglect the hopping terms in the simulation. Although the inclusion of the hopping terms increases the error, it is difficult to separate the effects of the numerical error and the hopping terms. For more detailed analysis of the effect of hopping, the TDSE solver should be improved. The frequency conversion and the phase-shift gate should be implemented in experiments by modulating the DC voltage on the electrodes of the surface electrode trap [20]. The parameters used in the numerical simulation are comparable to those used in Ref. [20] and thus our proposal should be experimentally feasible. However, because the analytical formula does not rely on the adiabatic approximation, we can adopt a faster frequency conversion in the future. We expect that the proposed method will contribute to the scaling up of the CV encoded trapped-ion quantum computers as well as the analog quantum simulator.

#### ACKNOWLEDGMENTS

The author thanks Kaoru Yamanouchi for his valuable comments on the present study and Takashi Mukaiyama and Tomoya Okino for their helpful discussion on experimental aspects. This work was supported by JST-CREST Grant No. JPMJCR23I7.

#### Appendix A: Hamiltonian of a chain of trapped ions

We consider  $M$  trapped ions and their local modes along  $X$  axis and assume that, if we neglect the Coulomb coupling, the secular frequency of each mode is given by  $\omega_{0,j}$ . Then, the total Hamiltonian for  $M$  harmonic oscillators interacting through the Coulomb coupling is given by [21]

$$\begin{aligned}H_0 = \sum_j & \left( \frac{P_j^2}{2m} + \frac{mX_j^2}{2} \left( \omega_{0,j}^2 - \sum_{k \neq j} \frac{e^2}{4\pi\epsilon_0 d_{j,k}^3 m} \right) \right) \\ & + \sum_{j > k} \frac{e^2}{4\pi\epsilon_0 d_{j,k}^3} X_j X_k,\end{aligned}\quad (A1)$$

where  $m$  is the mass of an ion and  $d_{j,k}$  is the distance between the equilibrium position of the  $j$ th and the  $k$ th modes. In order to simplify the notation, we redefine the secular frequency of the  $j$ th mode as  $\omega_j \equiv \sqrt{\omega_{0,j}^2 - \sum_{k \neq j} e^2 / (4\pi\epsilon_0 d_{j,k}^3 m)}$ . By defining the scaled coordinate and momentum as  $x_j = X_j / x_{0,j}$  and

$p_j = P_j/p_{0,j}$ , respectively, with  $x_{0,j} = \sqrt{\hbar/(m\omega_j)}$  and  $p_{0,j} = \sqrt{\hbar m\omega_j}$ , Eq. A1 is rewritten as

$$\begin{aligned} H_0 &= \sum_j \frac{\hbar\omega_j}{2} (p_j^2 + x_j^2) + \sum_{j>k} \hbar\kappa_{j,k} x_j x_k \\ &\simeq \sum_j \frac{\hbar\omega_j}{2} (p_j^2 + x_j^2) + \sum_{j>k} \frac{\hbar\kappa_{j,k}}{2} (x_j x_k + p_j p_k) \quad (\text{A2}) \\ &= \sum_j \hbar\omega_j \left( a_j^\dagger a_j + \frac{1}{2} \right) + \sum_{j>k} \frac{\hbar\kappa_{j,k}}{2} \left( a_j^\dagger a_k + a_j a_k^\dagger \right). \quad (\text{A3}) \end{aligned}$$

where  $\kappa_{j,k} = e^2/(4\pi\epsilon_0 d_{j,k}^3 m \sqrt{\omega_j \omega_k})$ . The second line is obtained by applying the rotating-wave approximation and the third line is obtained by defining  $x_j = (a_j^\dagger + a_j)/\sqrt{2}$  and  $p_j = i(a_j^\dagger - a_j)/\sqrt{2}$ .

For the FC, what we can modulate is the bare frequency  $\omega_{0,j}$  as  $\omega_{0,j}(t)$  and we define  $\omega_j(t) \equiv \sqrt{\omega_{0,j}(t) - \sum_{k \neq j} e^2/(4\pi\epsilon_0 d_{j,k}^3 m)}$  as the time-dependent frequency of the TDHO. Therefore, the Hamiltonian can be written as

$$\begin{aligned} H(t) &= \sum_j \left( \frac{P_j^2}{2m} + \frac{m}{2} \omega_j^2(t) X_j^2 \right) + \sum_{j>k} \frac{e^2}{4\pi\epsilon_0 d_{j,k}^3} X_j X_k \\ &= H_0 + \sum_j \frac{\hbar\Omega_j^2(t)}{2\omega_j} x_j^2 \quad (\text{A4}) \end{aligned}$$

$$= H_0 + \sum_j \frac{\hbar\Omega_j^2(t)}{4\omega_j} (a_j^\dagger + a_j)^2, \quad (\text{A5})$$

where we defined the difference of the squared frequency as  $\Omega_j^2(t) \equiv \omega_j^2(t) - \omega_j^2 = \omega_{0,j}^2(t) - \omega_{0,j}^2$ .

## Appendix B: Basis change

When we consider the TDHO with  $H(t) = P^2/(2m) + m\omega^2(t)X^2/2$  and the time evolution from  $\omega(t_i) = \omega_i$  to  $\omega(t_f) = \omega_f$ , the scaled coordinates should be defined at  $t_i$  and  $t_f$  as  $x_{\omega_i} = \sqrt{m\omega_i/\hbar}X$  and  $x_{\omega_f} = \sqrt{m\omega_f/\hbar}X$ , respectively, and are related as

$$x_{\omega_f} = \sqrt{\frac{\omega_f}{\omega_i}} x_{\omega_i} \equiv r_\omega x_{\omega_i}, \quad (\text{B1})$$

$$p_{\omega_f} = \sqrt{\frac{\omega_i}{\omega_f}} p_{\omega_i} \equiv r_\omega^{-1} p_{\omega_i}. \quad (\text{B2})$$

By denoting the lowering operator at each time as  $a_{\omega_i}$  and  $a_{\omega_f}$ , their relation can be obtained as

$$\begin{aligned} a_{\omega_i} &= \frac{1}{\sqrt{2}} (x_{\omega_i} + i p_{\omega_i}) \\ &= \frac{1}{2} \left( r_\omega^{-1} (a_{\omega_f}^\dagger + a_{\omega_f}) - r_\omega (a_{\omega_f}^\dagger - a_{\omega_f}) \right) \\ &= \frac{r_\omega + r_\omega^{-1}}{2} a_{\omega_f} - \frac{r_\omega - r_\omega^{-1}}{2} a_{\omega_f}^\dagger \\ &= a_{\omega_f} \cosh r - a_{\omega_f}^\dagger \sinh r, \end{aligned} \quad (\text{B3})$$

where we defined  $r = \log r_\omega$ . Therefore, the basis change can be regarded as the squeezing with  $r$  the squeezing strength.

## Appendix C: The Lewis–Riesenfeld theory

The analytical solution of the TDHO was derived in the Heisenberg picture by Lewis and Riesenfeld [22] as we summarize below. Note that we adopt the notation used in Ref. [17]. If  $|\psi\rangle$  is the solution of the TDSE  $i\hbar\partial_t |\psi\rangle = H(t) |\psi\rangle$ ,  $I(t) |\psi\rangle$  is also the solution, where  $I(t)$  is a Hermitian operator satisfying

$$\frac{\partial I(t)}{\partial t} + \frac{1}{i\hbar} [I(t), H(t)] = 0, \quad (\text{C1})$$

and we denote  $I(t)$ ’s eigenvalues and eigenstates as  $\lambda_n$  and  $|\lambda_n, t\rangle$ , respectively. For the TDHO specified in Appendix B, by defining the invariant as

$$I(t) = \frac{(bp - m\dot{b}x)^2}{2m} + \frac{m}{2} \left( \frac{\omega_i}{b} \right)^2 x^2, \quad (\text{C2})$$

where  $b(t)$  satisfies

$$\ddot{b} + \omega^2(t)b - \frac{\omega_i^2}{b^3} = 0 \quad (\text{C3})$$

$$\iff \omega(t) = \sqrt{\left( \frac{\omega_i^2}{b^3} - \ddot{b} \right) / b}, \quad (\text{C4})$$

the lowering and the raising operators for the eigenstates of  $I(t)$  can be defined respectively as

$$A(t) |\lambda_n, t\rangle = \sqrt{n} |\lambda_{n-1}, t\rangle, \quad (\text{C5})$$

$$A^\dagger(t) |\lambda_n, t\rangle = \sqrt{n+1} |\lambda_{n+1}, t\rangle. \quad (\text{C6})$$

The eigenstates of  $I(t)$  are related to the solution of the TDSE as  $|\lambda_n, t\rangle e^{i(n+1/2)\Theta(t)}$ , where

$$\Theta(t) = - \int_{t_i}^t \frac{\omega_i}{b^2(t')} dt'. \quad (\text{C7})$$

We choose the initial condition of (C3) as  $b(t_i) = 1$  and  $\dot{b}(t_i) = 0$  so that  $I(t_i) = H(t_i)$  and  $A(t_i) = a_{\omega_i}$  are

satisfied. At the end of the propagation, the lowering operator is given as

$$A(t_f) = \eta(t_f)a_{\omega_f} + \zeta(t_f)a_{\omega_f}^\dagger, \quad (\text{C8})$$

where

$$\eta(t) = \frac{1}{2} \sqrt{\frac{\omega_i}{\omega_f}} \left( \frac{1}{b} + \frac{\omega_f}{\omega_i} b - i \frac{\dot{b}}{\omega_i} \right), \quad (\text{C9})$$

$$\zeta(t) = \frac{1}{2} \sqrt{\frac{\omega_i}{\omega_f}} \left( \frac{1}{b} - \frac{\omega_f}{\omega_i} b - i \frac{\dot{b}}{\omega_i} \right). \quad (\text{C10})$$

#### Appendix D: Frequency conversion

In order to derive the time evolution of the lowering operator in the Heisenberg picture, we expand the time-evolution operator as

$$U(t_f, t_i) = \sum_{n=0}^{\infty} e^{i(n+1/2)\Theta(t_f)} |\lambda_n, t_f\rangle \langle \lambda_n, t_i|. \quad (\text{D1})$$

By using Eq. (C5),  $A(t_f)$  can be related to  $a_{\omega_i}$  as

$$\begin{aligned} U(t_f, t_i) A(t_i) U^\dagger(t_f, t_i) \\ = U(t_f, t_i) \sum_{n=0}^{\infty} e^{-i(n+1/2)\Theta(t_f)} \sqrt{n} |\lambda_{n-1}, t_i\rangle \langle \lambda_n, t_f| \\ = e^{-i\Theta(t_f)} \sum_{n=0}^{\infty} \sqrt{n} |\lambda_{n-1}, t_f\rangle \langle \lambda_n, t_f| = e^{-i\Theta(t_f)} A(t_f) \\ \implies A(t_f) = e^{i\Theta(t_f)} U(t_f, t_i) a_{\omega_i} U^\dagger(t_f, t_i). \end{aligned} \quad (\text{D2})$$

Combining this with Eq. (C8), we obtain

$$\begin{aligned} A(t_f) &= \eta(t_f)a_{\omega_f} + \zeta(t_f)a_{\omega_f}^\dagger \\ &= e^{i\Theta(t_f)} U(t_f, t_i) a_{\omega_i} U^\dagger(t_f, t_i), \end{aligned} \quad (\text{D3})$$

from which we can relate the time evolution of  $a_{\omega_f}$  with  $a_{\omega_i}$  as

$$\begin{aligned} \eta(t_f)a_{\omega_f}(t_f) + \zeta(t_f)a_{\omega_f}^\dagger(t_f) &= e^{i\Theta(t_f)} a_{\omega_i} \\ \implies a_{\omega_f}(t_f) &= \eta^* e^{i\Theta(t_f)} a_{\omega_i} - \zeta e^{-i\Theta(t_f)} a_{\omega_i}^\dagger, \end{aligned} \quad (\text{D4})$$

where we used  $a_{\omega_f}(t) = U^\dagger(t, t_i) a_{\omega_f} U(t, t_i)$ . By denoting the lowering and the raising operators by a vector  $\mathbf{a}_\omega = [a_\omega, a_\omega^\dagger]^T$ , Eq. (D4) can be summarized using a transformation matrix  $S_{if}$  as  $\mathbf{a}_{\omega_f}(t_f) = S_{if} \mathbf{a}_{\omega_i}$ , where

$$S_{if} = \begin{bmatrix} \eta^* e^{i\Theta(t_f)} & -\zeta e^{-i\Theta(t_f)} \\ -\zeta^* e^{i\Theta(t_f)} & \eta e^{-i\Theta(t_f)} \end{bmatrix}. \quad (\text{D5})$$

Finally, by applying Eq. (B3) to Eq. (D4), the time evolution of  $a_{\omega_i}$  can be obtained as

$$\begin{aligned} a_{\omega_i}(t_f) &= a_{\omega_f}(t_f) \cosh r - a_{\omega_f}^\dagger(t_f) \sinh r \\ &= (\eta^* \cosh r + \zeta^* \sinh r) e^{i\Theta(t_f)} a_{\omega_i} \\ &\quad - (\eta \sinh r + \zeta \cosh r) e^{-i\Theta(t_f)} a_{\omega_i}^\dagger. \end{aligned} \quad (\text{D6})$$

#### Appendix E: Adiabatic condition

Although the adiabatic condition does not need to be satisfied for FC, the parameters adopted in III are in the adiabatic regime as shown below. For a system driven by a non-periodic time-dependent potential, the adiabatic condition is given as [28]

$$\sum_{m \neq n} \frac{\hbar |\langle m; t | \dot{H} | n; t \rangle|}{|E_m(t) - E_n(t)|^2} \ll 1, \quad (\text{E1})$$

where  $E_n(t)$  and  $|n; t\rangle$  are the  $n$ th eigen energy and the eigen vector of the instantaneous Hamiltonian, i.e.,  $H(t) |n; t\rangle = E_n(t) |n; t\rangle$ . When we consider a single mode, the Hamiltonian of FC( $\omega_i \rightarrow \omega'$ ) and its time derivative are given respectively by

$$H(t) = \frac{\hbar \omega_i}{2} (p^2 + x^2) + \frac{\hbar(\omega^2(t) - \omega_i^2)}{2\omega_i} x^2 \quad (\text{E2})$$

$$\dot{H} = \frac{\hbar \omega(t) \dot{\omega}}{\omega_i} x^2, \quad (\text{E3})$$

and the instantaneous eigen energy is given by  $E_n(t) = \hbar \omega(t)(n + 1/2)$ . In order to calculate  $|\langle m; t | \dot{H} | n; t \rangle| \propto |\langle m; t | x^2 | n; t \rangle|$ , we need to change the basis using Eq. (B1) as

$$x = \sqrt{\frac{\omega_i}{\omega(t)}} x_t. \quad (\text{E4})$$

By defining the lowering and the raising operators with respect to  $|n; t\rangle$ , Eq. (E1) can be rewritten as

$$\sum_{m \neq n} \frac{|\dot{\omega} \langle m; t | (a_t^\dagger + a_t)^2 | n; t \rangle|}{2\omega^2(t)(m - n)^2} \ll 1. \quad (\text{E5})$$

In the numerator of Eq. (E5), only the terms satisfying  $|m - n| = 2$  are finite and therefore we only require the terms in the sum in Eq. (E5) with large  $n$  to satisfy the following,

$$\frac{\sqrt{(n+1)(n+2)} |\dot{\omega}|}{8\omega^2(t)} \simeq \frac{n |\dot{\omega}|}{8\omega^2(t)} \ll 1. \quad (\text{E6})$$

For a smooth function such as  $\omega(t)$  shown in Fig. 1,  $|\dot{\omega}|$  becomes its maximum at  $t = T_{\text{FC}}/2$ . For  $b(t)$  defined using Eqs. (16) or (17),  $\ddot{b}(T_{\text{FC}}/2) = 0$  is satisfied and so we approximate Eq. (C4) as  $\omega(t) \simeq \omega_i/b^2$  around  $t = T_{\text{FC}}/2$ . Consequently, the time derivative is given as

$$\dot{\omega} \left( \frac{T_{\text{FC}}}{2} \right) = -2\omega_i \dot{b} b^{-3} = -2\omega_i \left( \mp \frac{g\sigma}{\sqrt{\pi} T_{\text{FC}}} \right) \left( 1 \mp \frac{g}{2} \right)^{-3}, \quad (\text{E7})$$

where the minus (plus) sign in parentheses is for the up (down) conversion. For the parameters specified in III, the left-hand side of Eq. (E6) is obtained as  $6 \times 10^{-4} n$  for FC( $\omega_h \rightarrow \omega_m$ ) and  $7 \times 10^{-4} n$  for FC( $\omega_l \rightarrow \omega_m$ ). Therefore,

the adiabatic condition is satisfied even when  $n$  is as large as a few hundred. Further simplification can be made when  $g$  is small. Because  $b^{-3} \simeq 1$  for small  $g$ , Eq. (E6) can be rewritten as

$$\frac{|g|\sigma}{4\sqrt{\pi}\omega(T_{\text{FC}}/2)T_{\text{FC}}}n \ll 1, \quad (\text{E8})$$

where  $\omega(T_{\text{FC}}/2)T_{\text{FC}}/(2\pi) \simeq 9$  is the number of oscillation cycles within  $T_{\text{FC}}$ . Therefore, for a small value of  $|g|$ , even when we decrease the duration down to the single oscillation period, i.e.,  $\omega(T_{\text{FC}}/2)T_{\text{FC}}/(2\pi) \simeq 1$ , the adiabatic condition is still valid if  $n$  is several dozen or smaller.

---

[1] D. Gottesman, A. Kitaev, and J. Preskill, *Physical Review A: Atomic, Molecular, and Optical Physics* **64**, 012310 (2001).

[2] P. T. Cochrane, G. J. Milburn, and W. J. Munro, *Physical Review A* **59**, 2631 (1999).

[3] H. Puterman, K. Noh, C. T. Hann, G. S. MacCabe, S. Aghaeimeibodi, R. N. Patel, M. Lee, W. M. Jones, H. Moradinejad, R. Rodriguez, N. Mahuli, J. Rose, J. C. Owens, H. Levine, E. Rosenfeld, P. Reinhold, L. Moncelsi, J. A. Alcid, N. Alidoust, P. Arrangoiz-Arriola, J. Barnett, P. Bienias, H. A. Carson, C. Chen, L. Chen, H. Chinkezian, E. M. Chisholm, M. H. Chou, A. Clerk, A. Clifford, R. Cosmic, A. V. Curiel, E. Davis, L. DeLorenzo, J. M. D'Ewart, A. Diky, N. D'Souza, P. T. Dumitrescu, S. Eisenmann, E. Elkhouly, G. Evenbly, M. T. Fang, Y. Fang, M. J. Fling, W. Fon, G. Garcia, A. V. Gorshkov, J. A. Grant, M. J. Gray, S. Grimberg, A. L. Grimsmo, A. Haim, J. Hand, Y. He, M. Hernandez, D. Hover, J. S. Hung, M. Hunt, J. Iverson, I. Jarrige, J. C. Jaskula, L. Jiang, M. Kalaei, R. Karabalin, P. J. Karalekas, A. J. Keller, A. Khalajhedayati, A. Kubica, H. Lee, C. Leroux, S. Lieu, V. Ly, K. V. Madrigal, G. Marcaud, G. McCabe, C. Miles, A. Milsted, J. Minguzzi, A. Mishra, B. Mukherjee, M. Naghiloo, E. Oblepias, G. Ortuno, J. Pagdilao, N. Pancotti, A. Panduro, J. P. Paquette, M. Park, G. A. Peairs, D. Perello, E. C. Peterson, S. Ponte, J. Preskill, J. Qiao, G. Refael, R. Resnick, A. Retzker, O. A. Reyna, M. Runyan, C. A. Ryan, A. Sahmoud, E. Sanchez, R. Sanil, K. Sankar, Y. Sato, T. Scaffidi, S. Siavoshi, P. Sivarajah, T. Skogland, C. J. Su, L. J. Swenson, S. M. Teo, A. Tomada, G. Torlai, E. A. Wollack, Y. Ye, J. A. Zerrudo, K. Zhang, F. G. Brandão, M. H. Matheny, and O. Painter, *Nature* **638**, 927 (2025).

[4] D. Porras and J. I. Cirac, *Physical Review Letters* **93**, 263602 (2004).

[5] K. Toyoda, Y. Matsuno, A. Noguchi, S. Haze, and S. Urabe, *Physical Review Letters* **111**, 160501 (2013).

[6] O. Katz and C. Monroe, *Physical Review Letters* **131**, 033604 (2023).

[7] R. J. MacDonell, C. E. Dickerson, C. J. Birch, A. Kumar, C. L. Edmunds, M. J. Biercuk, C. Hempel, and I. Kassal, *Chemical Science* **12**, 9794 (2021).

[8] V. C. Olaya-Agudelo, B. Stewart, C. H. Valahu, R. J. MacDonell, M. J. Millican, V. G. Matsos, F. Scuccimarra, T. R. Tan, and I. Kassal, *Physical Review Research* **7**, 023215 (2025).

[9] C. Flühmann, T. L. Nguyen, M. Marinelli, V. Negnevitsky, K. Mehta, and J. P. Home, *Nature* **566**, 513 (2019).

[10] B. de Neeve, T. L. Nguyen, T. Behrle, and J. P. Home, *Nature Physics* **18**, 296 (2022).

[11] P. Campagne-Ibarcq, A. Eickbusch, S. Touzard, E. Zalys-Geller, N. E. Frattini, V. V. Sivak, P. Reinhold, S. Puri, S. Shankar, R. J. Schoelkopf, L. Frunzio, M. Mirrahimi, and M. H. Devoret, *Nature* **584**, 368 (2020).

[12] V. V. Sivak, A. Eickbusch, B. Royer, S. Singh, I. Tsitsios, S. Ganjam, A. Miano, B. L. Brock, A. Z. Ding, L. Frunzio, S. M. Girvin, R. J. Schoelkopf, and M. H. Devoret, *Nature* **616**, 50 (2023).

[13] V. G. Matsos, C. H. Valahu, M. J. Millican, T. Navickas, X. C. Kolesnikow, M. J. Biercuk, and T. R. Tan, *Nature Physics* (2025) <https://doi.org/10.1038/s41567-025-03002-8>.

[14] S. Debnath, N. M. Linke, S. T. Wang, C. Figgatt, K. A. Landsman, L. M. Duan, and C. Monroe, *Physical Review Letters* **120**, 073001 (2018).

[15] R. Ohira, S. Kume, K. Takayama, S. Muralidharan, H. Takahashi, and K. Toyoda, *Physical Review A* **103**, 012612 (2021).

[16] S. A. Moses, C. H. Baldwin, M. S. Allman, R. Ancona, L. Ascarrunz, C. Barnes, J. Bartolotta, B. Bjork, P. Blanchard, M. Bohn, J. G. Bohnet, N. C. Brown, N. Q. Burdick, W. C. Burton, S. L. Campbell, J. P. Campora, C. Carron, J. Chambers, J. W. Chan, Y. H. Chen, A. Chernoguzov, E. Chertkov, J. Colina, J. P. Curtis, R. Daniel, M. Decross, D. Deen, C. Delaney, J. M. Dreiling, C. T. Ertsgaard, J. Esposito, B. Estey, M. Fabrikant, C. Figgatt, C. Foltz, M. Foss-Feig, D. Francois, J. P. Gaebler, T. M. Gatterman, C. N. Gilbreth, J. Giles, E. Glynn, A. Hall, A. M. Hankin, A. Hansen, D. Hayes, B. Higashi, I. M. Hoffman, B. Horning, J. J. Hout, R. Jacobs, J. Johansen, L. Jones, J. Karcz, T. Klein, P. Lauria, P. Lee, D. Liefer, S. T. Lu, D. Lucchetti, C. Lytle, A. Malm, M. Matheny, B. Mathewson, K. Mayer, D. B. Miller, M. Mills, B. Neyenhuis, L. Nugent, S. Olson, J. Parks, G. N. Price, Z. Price, M. Pugh, A. Ransford, A. P. Reed, C. Roman, M. Rowe, C. Ryan-Anderson, S. Sanders, J. Sedlacek, P. Shevchuk, P. Siegfried, T. Skripka, B. Spaun, R. T. Sprenkle, R. P. Stutz, M. Swallows, R. I. Tobey, A. Tran, T. Tran, E. Vogt, C. Volin, J. Walker, A. M. Zolot, and J. M. Pino, *Physical Review X* **13**, 041052 (2023).

[17] H. K. Lau and D. F. James, *Physical Review A - Atomic, Molecular, and Optical Physics* **85**, 062329 (2012).

[18] C. Shen, Z. Zhang, and L. M. Duan, *Physical Review Letters* **112**, 050504 (2014).

[19] R. Ohira, S. Kume, and K. Toyoda, *Physical Review A* **106**, 042603 (2022).

[20] M. Mielenz, H. Kalis, M. Wittemer, F. Hakelberg, U. Warring, R. Schmied, M. Blain, P. Maunz, D. L. Moehring, D. Leibfried, and T. Schaetz, *Nature Communications* **7**, 1 (2016).

[21] T. Nishi, K. Yamanouchi, R. Saito, and T. Mukaiyama, *Physical Review A* **111**, 022401 (2025).

- [22] H. R. Lewis and W. B. Riesenfeld, *Journal of Mathematical Physics* **10**, 1458 (1969).
- [23] J. Haegeman, J. I. Cirac, T. J. Osborne, I. PiÅorn, H. Verschelde, and F. Verstraete, *Physical Review Letters* **107**, 070601 (2011).
- [24] J. Haegeman, C. Lubich, I. Oseledets, B. Vandereycken, and F. Verstraete, *Physical Review B* **94**, 165116 (2016).
- [25] W. Guan, P. Bao, J. Peng, Z. Lan, and Q. Shi, *Journal of Chemical Physics* **161**, 122501 (2024).
- [26] C. K. Hong, Z. Y. Ou, and L. Mandel, *Physical Review Letters* **59**, 2044 (1987).
- [27] I. Rojkov, P. M. Röggla, M. Wagener, M. Fontboté-Schmidt, S. Welte, J. Home, and F. Reiter, *Physical Review Letters* **133**, 100601 (2024).
- [28] D. Comparat, *Physical Review A* **80**, 012106 (2009).